MHD CHANNEL FLOW IN AN INHOMOGENEOUS MAGNETIC FIELD. PART 3. NUMERICAL MODELING OF THE MEAN FLOW

F. Dubois, J. Etay, O. Widlund, Y. Delannoy
CNRS-EPM (Madylam), ENSHMG, BP 95, F-38402 St Martin d'Hères, France
(etay@grenoble.cnrs.fr)

Introduction. The paper presents numerical simulations of the Ilmenau Galinstan experimental loop, featuring a channel-flow test section in an inhomogeneous transverse magnetic field. The simulations were performed using a special MHD module developed in-house for use with the commercial flow solver Fluent. The MHD module includes the necessary functionality for accurately solving the electromagnetic equations. It also implements powerful models for MHD turbulence, and a recently proposed wall function treatment for laminar MHD boundary layers. We first discuss the implementation of the laminar MHD wall functions, and then present numerical simulations of the Ilmenau loop. Tests with varying grid resolutions demonstrate the advantages of the new wall treatment, also in an inhomogeneous magnetic field. Comparison of numerical predictions and measurements helps our understanding of the flow in the experimental loop. Many of the observed differences can be related to experimental difficulties; others are more difficult to explain, and should be studied further.

1. Wall functions for laminar MHD boundary layers. In order to reduce the computational cost of gridding laminar MHD boundary layers, we have implemented a wall function treatment proposed by Widlund [1]. The wall functions depend only on local variables, and are valid for all walls, regardless of their orientation relative to the magnetic field. The method is, therefore, well suited for modeling of flows in complicated geometries and inhomogeneous magnetic fields, and it is relatively easy to implement in existing flow solvers, such as Fluent.

In the vicinity of a wall, all vector quantities can be split into components normal (n) and parallel (p) to the wall. Neglecting the convection terms and wall-parallel diffusion, the momentum equation can be integrated analytically in the wall-normal direction. This yields a "wall function" relating the wall-parallel velocity in the first computational node to the wall shear stress τ and various local variables; see [1] for details. The wall function is used in the solution of the momentum equations to specify the wall shear stress as a function of the velocity in the first node and other local variables. The same velocity profile is used to compute $\mathbf{U} \times \mathbf{B}$ in the near-wall cells (for use in the electric potential source term and for computing the electric current density).

For the case of a fully developed rectangular channel flow, the Fluent implementation of the laminar MHD wall functions reproduces almost exactly the same results as those found by Widlund. The accuracy of the predicted pressure drop and friction coefficients were in the order of 1%, and essentially independent of the resolution of the Hartmann layers.

Taking advantage of the geometrical flexibility offered by Fluent, the wall functions have been tested also for the case of a fully developed circular pipe flow in a transverse magnetic field (non-conducting walls). This case notes the fact that the wall treatment can be applied independently of the orientation of the wall relative to the magnetic field. The results are validated against the analytic

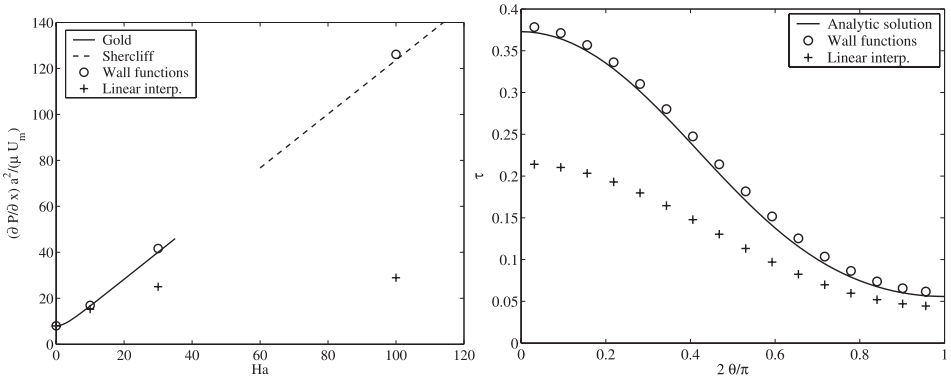

Fig. 1. Performance of MHD wall functions for a fully developed pipe flow.

solution by Gold [2] and the asymptotic solution by Shercliff [3]. The Fluent geometry models half of the circular cross-section, with a symmetry plane at $y = 0$; the flow is along the x-axis, and the magnetic field is in the y-direction. The cylindrical grid is uniform, with 10 cells in the radial direction and 32 in the azimuthal direction.

Figure 1 compares numerical predictions and theoretical values. The left pane shows a non-dimensional pressure drop. The wall function predictions slightly over-estimate the pressure drop, but the relative error remains virtually independent of the Hartmann number. The right pane shows local shear stress predictions for $\mathrm{Ha} = 30$. The magnetic field is perpendicular to the wall for $\theta = 0$ (Hartmann layer), and parallel to the wall when $\theta = \pi/2$.

2. Numerical model of the Ilmenau loop. The Ilmenau Galinstan experimental loop is described in detail in a companion paper by Andrejews and Kolesnikov [4]. The horizontal test section is 455 mm long, with a cross-section 100 mm wide and 20 mm high. The inlet velocity profile is shaped by a honeycomb. A 30 mm long permanent magnet placed 155 mm downstream of the test section inlet generates a vertical magnetic field, with a maximum flux density of $0,504$ T. The strong field gradients at the entry and exit of the magnet will create a characteristic M-shaped velocity profile, with strong wall jets along the vertical side walls. Thin Hartmann boundary layers develop along the horizontal walls inside the magnetic field. The test case considered here has a Reynolds number of 4000 (based on the channel height). The Hartmann number is 400 (based on the maximum flux density), and the corresponding Hartmann length scale is $\delta_{\mathrm{H}} = \sqrt{\mu/\sigma}/B_{\max} = 50$ μm. This gives the interaction parameter $N = \mathrm{Ha}^2/\mathrm{Re} = 40$.

The numerical model is illustrated in Fig. 2. The flow is in the x-direction, and the magnetic field is in the z-direction. We model only the upper half of the the channel, with a horizontal symmetry plane at $z = 0$.

Calculations were performed with two different grids in order to test the performance of the wall function treatment. The two grids differ only in the resolution near the Hartmann wall. In the coarse grid the near-wall grid size is 1 mm, so that the Hartmann boundary layer is not at all resolved. The finer grid uses exponential grid refinement to resolve the Hartmann layer, and the near-wall grid size is only 8.9 μm. For both grids, the grid size near the side walls is 16 μm to assure a good resolution of the wall jets. The coarse grid has about 32000 cells, and the fine grid about 80000.

Based on actual measurements, the inlet velocity profile is assumed a function of y (channel width), but uniform over the height of the channel. is based on the

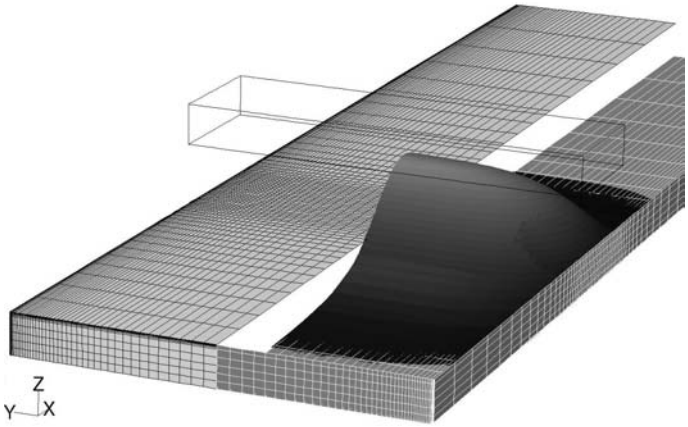

Fig. 2. Illustration of model geometry (upper half of the channel), gridding and magnetic field distribution, as seen from the inlet.

honeycomb cell size. The outlet uses a constant pressure boundary condition. For the electric potential, we assume $\partial\phi/\partial n = 0$ at the inlet boundary and $\phi = 0$ at the outlet. Test calculations showed that the choice of electric boundary conditions at the inlet and outlet boundaries has no effect on the results near the magnet. All walls are assumed electrically isolating, so that $\partial\phi/\partial n = 0$. The vertical side walls use standard no-slip velocity boundary conditions. For the horizontal walls, simulation were performed both with standard no-slip conditions and with the new MHD wall functions. The vertical component of the magnetic field distribution is based on measurements, while the horizontal components are assumed small and neglected.

The results shown here are from laminar steady-state calculations; at this Reynolds number, the flow from the inlet honeycomb can be only very weakly turbulent, and any turbulence is effectively damped in the vicinity of the magnetic field.

2.1. Performance of the wall functions. Three different simulations were performed to evaluate the performance of the wall functions: (i) fine grid with standard no-slip boundary conditions; (ii) coarse grid with standard no-slip boundary conditions; (iii) coarse grid with wall functions. The results are compared in Fig. 3. With the wall functions, the results are as accurate on the coarse grid, as with the

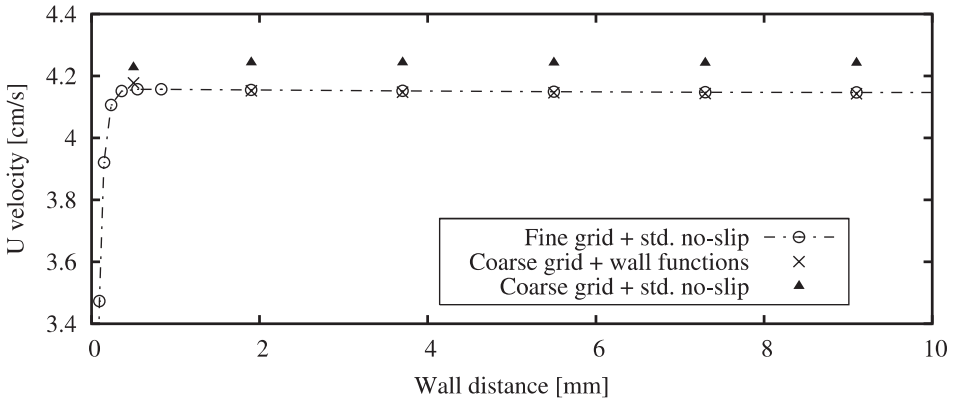

Fig. 3. Performance of wall functions, compared to standard boundary conditions. Velocity profile in the Hartmann layer, at $x = 0$, $y = 25$ mm.

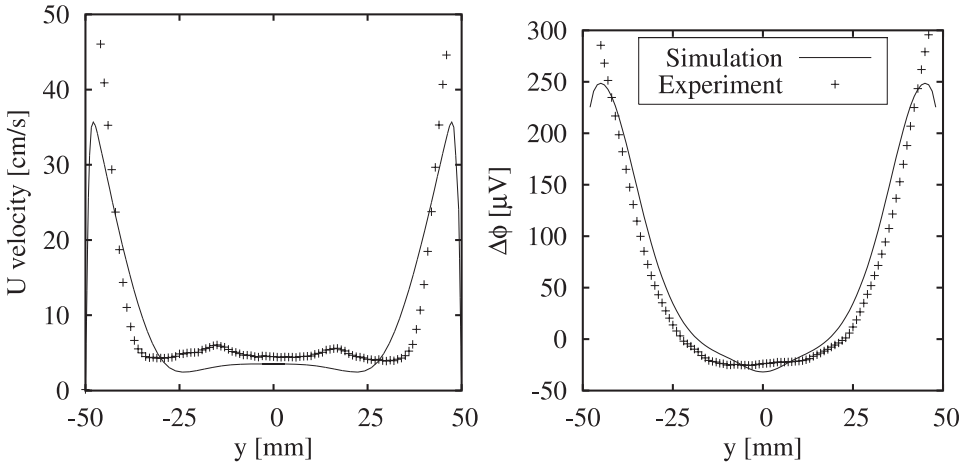

Fig. 4. Velocities (left) measured by the Vives probe at $x = 195$ mm (downstream of the magnet), and potential differences (right) measured by the potential probe at $x = 0$ (center of magnet). Symmetry plane, $z = 0$.

standard boundary conditions on a finer grid.

2.2. Comparison with experimental results. Measurements were performed using both a Vives probe and a potential probe. The Vives probe is calibrated in the absence of an external field, so the measured velocities can be expected to be accurate only some distance away from the magnet. The potential probe, on the other hand, measures the potential gradient created by the external magnetic field, and will give a strong signal only in the close vicinity of the magnet. The reconstruction of velocity from the signal of the potential probe assumes that the electric current is weak, so that

$$\frac{\partial \phi}{\partial y} = -\frac{J_y}{\sigma} - U_x B_z \approx -U_x B_z.$$

In a strongly inhomogeneous case at hand, the simulation results can be used to show that this hypothesis is poor almost everywhere. We have therefore chosen to compare potential differences directly, rather than the reconstructed velocities. Numerically predicted potential differences were taken between two discrete points at a distance of 4 mm, to emulate the finite size of the potential probe. Fig. 4 shows examples of measurements compared with the numerical predictions. Some of the differences observed can be related to experimental difficulties, especially close to the walls. Other discrepancies are more difficult to explain, and should be studied further.

REFERENCES

1. O. Widlund. Wall functions for numerical modeling of laminar MHD flows. *Eur. J. Mech. B/Fluids*, vol. 22 (2003), pp. 221–237.

2. R. R. Gold. Magnetohydrodynamic pipe flow. Part 1. *Journal of Fluid Mechanics*, vol. 13 (1962), pp. 505–512.

3. J. A. Shercliff. Magnetohydrodynamic pipe flow. Part 2. High Hartmann number. *Journal of Fluid Mechanics*, vol. 13 (1962), pp. 513–518.

4. O. Andrejews and Y. Kolesnikov. MHD channel flow of liquid metal in an inhomogeneous magnetic field, Part 1: Experiment. In *Proceedings of the Sixth PAMIR Conference, June 27–July 1, 2005* (PAMIR, Rigas Jurmala, Latvia).